Clin Neuroradiol (2019) 29:631–638
https://doi.org/10.1007/s00062-018-0706-0

ORIGINAL ARTICLE

Improved Brachial Plexus Visualization Using an Adiabatic iMSDE-Prepared STIR 3D TSE

Elisabeth Klupp[1] · Barbara Cervantes[2] · Nico Sollmann[1] · Franziska Treibel[2] · Dominik Weidlich[2] · Thomas Baum[1] · Ernst J. Rummeny[2] · Claus Zimmer[1] · Jan S. Kirschke[1] · Dimitrios C. Karampinos[2]

Received: 26 March 2018 / Accepted: 3 July 2018 / Published online: 23 July 2018

Abstract

Purpose The close proximity of blood vessels to the brachial plexus nerves can confound nerve visualization in conventional fat-suppressed 3D T2-weighted sequences. Vessel suppression can be accomplished by means of motion-sensitizing preparation. The aim of this study was to qualitatively and semi-quantitatively evaluate short tau inversion recovery (STIR) 3D turbo spin echo (TSE) in conjunction with an adiabatic T2 preparation incorporating motion sensitization for magnetic resonance neurography (MRN) of the brachial plexus in a clinical routine setting.

Methods The MRN of the brachial plexus was performed in 22 patients (age 45.5 ± 20.3 years) with different clinical implications using the proposed improved motion-sensitized driven equilibrium (iMSDE) STIR 3D TSE and the STIR 3D TSE. Images were evaluated regarding image quality, overall artifacts, artifacts caused by vessel signal, signal homogeneity, visibility of small nerves and signal contrast. Furthermore, signal-to-noise ratios (aSNR), nerve muscle contrast to noise ratios (aNMCNR) and nerve vessel contrast to noise ratios (aNVCNR) were calculated and compared.

Results The incorporation of motion sensitization in the T2 preparation resulted in robust blood suppression across subjects, leading to significantly higher aNVCNRs ($p < 0.001$) and aNMCNRs ($p < 0.05$), increased conspicuousness of the nerves, better vessel suppression and image quality and less artifacts compared with STIR 3D TSE ($p < 0.001$).

Conclusion The incorporation of the proposed adiabatic iMSDE-based motion sensitization was shown to provide robust blood suppression of vessels in close proximity to brachial plexus nerves. The use of STIR iMSDE 3D TSE can be considered for clinical MRN examinations of the brachial plexus.

Keywords MR neurography · Brachial plexus · 3-D Imaging · Fat suppression · Vessel suppression

Introduction

The brachial plexus is a network of nerves that run from the cervical spine to the upper extremities and supply motor and sensory innervation and can be involved in multiple disorders resulting in functional impairment of the upper limbs. The brachial plexus can be affected by a wide variety of pathologies, including traumatic injuries, spatially invasive lesions such as hematomas or tumors, inflammatory changes, infectious diseases and degenerative changes. The clinical differentiation of various plexopathies as well as from cervical spine-related abnormalities often provides a diagnostic challenge. Due to the deep location of the plexus, electrodiagnostic tests are difficult to perform; nerve roots and the proximal parts of the brachial plexus cannot be assessed properly and conduction abnormalities may be overlooked [1–4] leading to misinterpretation. Non-invasive magnetic resonance neurography (MRN) has become increasingly important in the diagnosis of brachial plexopathies and peripheral neuropathies [5–10].

The evaluation of the brachial plexus with MRI is conventionally carried out using 2D fat-suppressed T2-weighted imaging due to the high soft-tissue contrast and more recently using 3D fat-suppressed T2-weighted imaging due to the isotropic spatial resolution achieved with this technique [11, 12]. For fat suppression in 3D imaging, short tau inversion recovery (STIR) has been primarily used due to the severe magnetic field inhomogeneity effects in the

✉ Elisabeth Klupp
elisabeth.klupp@tum.de

[1] Department of Diagnostic and Interventional Neuroradiology, Klinikum rechts der Isar, Technical University of Munich, Ismaninger Str. 22, 81675 Munich, Germany

[2] Department of Diagnostic and Interventional Radiology, Klinikum rechts der Isar, Technical University of Munich, Ismaninger Str. 22, 81675 Munich, Germany

neck/shoulders region [13–16]. Although 3D techniques result in a high spatial resolution as well as in good delineation of the nerve structures, a major problem in plexus MRN remains the immediate proximity of blood vessels to the plexus. The conspicuous hyperintense vessel signal in T2-weighted images can confound and obscure the visualization of nerves and can therefore limit the diagnostic accuracy and significance of plexus MRN [17]. Vessel signal suppression in 3D MRN can be achieved by means of an additional motion-sensitizing T2 preparation prepulse. Improved motion-sensitized driven equilibrium (iMSDE) preparation has been shown to improve the visualization of nerves in various anatomical regions [18–21]. Another important consideration when employing a T2 preparation in MRN is the sensitivity of this preparation module to transmit B1 inhomogeneity effects. The purpose of the present work was to evaluate STIR 3D turbo spin echo (TSE) in conjunction with an adiabatic T2 preparation incorporating iMSDE-based motion sensitization (STIR iMSDE 3D TSE) for MRN of the brachial plexus in a clinical routine setting in comparison to STIR 3D TSE without a motion-sensitizing prepulse.

Material and Methods

Subjects

The study was approved by the local Institutional Review Board and conducted in accordance with the Committee for Human Research. A total of 22 patients, 8 women and 14 men (mean age: 45.5 ± 20.3 years; range: 18–87 years) participated in this study. These patients were referred mainly by the departments of neurology as well as neurosurgery with different clinical implications. All subjects gave written informed consent prior to their participation in the study.

MR Protocol

The STIR iMSDE 3D TSE sequence consists of a wide-band (WB) adiabatic inversion recovery pulse for robust fat suppression followed by a motion-sensitizing module for vessel suppression and a 3D TSE readout for isotropic-resolution imaging. The WB STIR pulse consists of an adiabatic hyperbolic secant inversion pulse with a length of 28.5 ms and a total bandwidth of 1820 Hz, effectively allowing fat suppression by means of inversion recovery that is robust to B1 and B0 inhomogeneities. The iMSDE preparation has a modified B_1-insensitive rotation (BIR)-4 pulse for a radiofrequency (RF) component, previously shown to increase robustness against B0 and transmit B1 effects when applied for T2 preparation [22–25]. The modified RF configuration consists of a BIR-4 pulse with gaps between the three RF components added to fit motion-sensitizing gradients, where the total duration of the BIR-4 RF pulse without gaps is 16 ms. The frequency sweep of the RF pulse has an amplitude of 3800 Hz. Fig. 1 shows the sequence diagram of the STIR iMSDE 3D TSE. The sensitivity of the applied modified BIR-4 pulse module to B1 and B0 errors was simulated with a Bloch simulation. The simulated parameters are as follows: T1/T2: 1200/70 ms, duration of T2 preparation = 32 ms, B1 = 13.5 µT, BIR-4 duration = 16 ms and BIR-4 frequency sweep = 3800 Hz. The performance was simulated for a frequency offset of ±500 Hz and from 50–120% of the nominal B1 field.

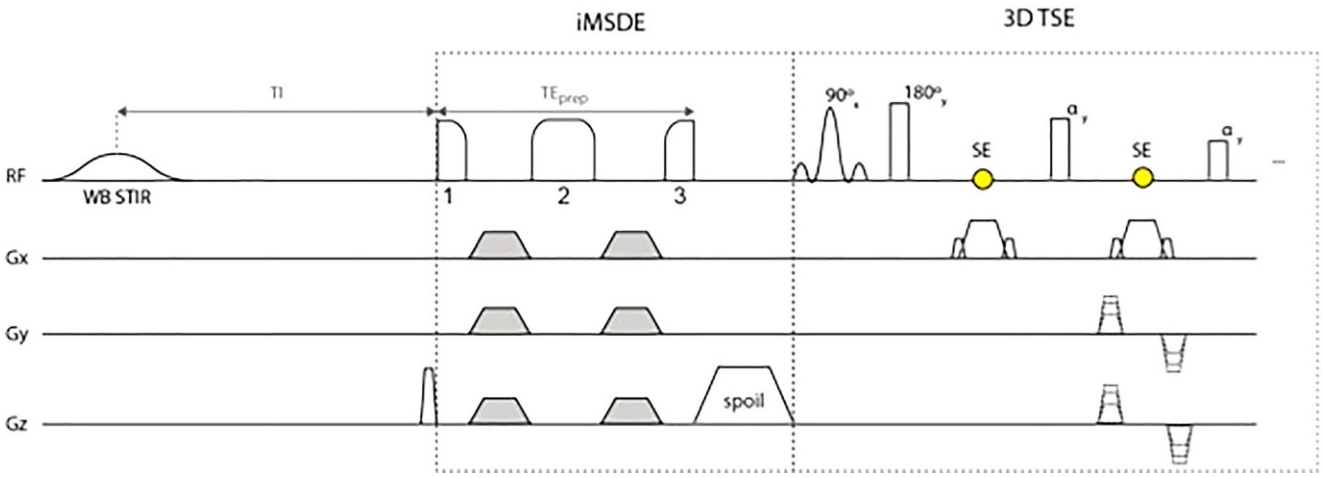

Fig. 1 Sequence diagram of short tau inversion recovery (STIR) improved motion-sensitized driven equilibrium (iMSDE) 3D turbo spin echo (TSE), which uses a wide band (WB) STIR pulse followed by an iMSDE preparation and a 3D TSE readout. The WB STIR pulse uses a hyperbolic-secant RF component for adiabatic inversion recovery and operates at maximum bandwidth for robust fat suppression in the presence of B1 and B0 inhomogeneities. After the inversion time (TI), the signal is excited by the first segment of the B1-insensitive rotation(BIR)-4 pulse. Motion-sensitizing gradients around the refocusing BIR-4 segment dephase vessel signals. Transverse magnetization is tipped-up by the pulse's restoration segment and residual transverse magnetization is removed with a spoiler gradient. Conventional 3D TSE readout follows

All acquisitions were performed with a 3T whole-body Philips scanner (Philips Ingenia, Best, The Netherlands) using a 16-channel torso coil, a 20-channel head-neck coil and the 12-channel embedded posterior coil. All patients received the standard MR protocol for the assessment of the brachial plexus consisting of the following sequences: coronal T1 weighted DIXON TSE with and without contrast agent; axial T2 weighted TSE and 3D STIR TSE. In addition to the standard sequences, the above described STIR iMSDE 3D TSE was applied. The STIR 3D TSE and STIR iMSDE 3D TSE acquisitions were performed coronally using the following sequence parameters: field of view: $250 \times 419 \times 220\,mm^3$; acquisition voxel: $1.49 \times 1.49 \times 1.50\,mm^3$; reconstruction voxel: $0.81 \times 0.81 \times 0.75\,mm^3$; repetition time/echo time: 2200 ms/121 ms; echo train length = 80; number of signal averages = 2 using phase cycling for removal of free induction decay artifacts; parallel imaging using sensitivity encoding (SENSE) with *P* reduction (RL) = 3; S reduction (AP) = 1.9; total scan duration: 05:47 min. The STIR 3D TSE images were acquired without and with the above described iMSDE prepulse (TE_{prep} = 32 ms; flow venc (cm/s) = (3) 1). Total scan time of the entire protocol was approximately 30 min.

Image Analysis and Evaluation

Apparent signal to noise ratio (aSNR), apparent nerve-muscle contrast to noise ratio (aNMCNR) and apparent nerve-vessel contrast to noise ratio (aNVCNR) were calculated form the source images of each patient. In accordance with Wang et al. aSNR, aNMCNR and aNVCNR were calculated using the following equations [26]:

$$\text{aSNR} = \frac{\text{Signal intensity (SI) nerve}}{\text{Standard deviation (SD) nerve}}$$

$$\text{aNMCNR} = \frac{\text{SI nerve} - \text{SI adjacent soft tissue}}{\text{SD nerve}}$$

$$\text{aNVCNR} = \frac{\text{SI nerve} - \text{SI adjacent vessel}}{\text{SD nerve}}$$

The aSNR and aNMCNR were measured in three different levels of the left brachial plexus following the C6 nerve: "proximal" close to the nerve root of C6, "center" at the level of the superior trunk (close to subclavian artery) and more "distal" at the level of the lateral cord. The aNVCNR was measured on representative perpendicular planes, which were placed in the "center" part close to the subclavian vessels. Regions of interests (ROIs) were placed in the proximal, center and distal areas of the left brachial plexus (following the C6 nerve), the adjacent soft tissue and the subclavian vessels. The ROIs for signal measurements were manually located.

Table 1 Semiquantitative assessment scoring system regarding image quality

	Score				
	1	2	3	4	5
Overall image quality	Very good to perfect quality	No compromise of diagnostic quality	Acceptable diagnostic quality	Unacceptable diagnostic quality	Nerves not distinguishable
Overall artifacts	No noticeable artifacts	Minimal artifacts. No compromise of diagnostic quality	Acceptable diagnostic quality	Unacceptable diagnostic quality	Nerve not distinguishable from surrounding
Vessel artifacts within plexus region	No vessel signal within plexus	No compromise of diagnostic quality	Acceptable diagnostic quality	Unacceptable diagnostic quality	Nerve not distinguishable from surrounding
Plexus signal homogeneity	Homogeneous	Homogeneous with minor hyperintensities	Homogeneous with major hyperintensities	Inhomogeneous	Nerve not distinguishable from surrounding
Visibility of small nerve branches	Perfect delineation	Good delineation with noticeable blurring	Delineation acceptable for clinical evaluation	Delineation insufficient for clinical evaluation	No distinction from background tissue
Contrast of nerve to surrounding tissue	Perfect contrast	Good contrast in most areas	Few areas with insufficient contrast	Many areas with insufficient contrast	Nerve not distinguishable from surrounding
Arterial suppression	Perfect suppression	Good suppression. No compromise of diagnostic quality	Moderate suppression. Acceptable diagnostic quality	Poor suppression. Unacceptable diagnostic quality	No distinction from background tissue
Venous suppression	Perfect suppression	Good suppression. No compromise of diagnostic quality	Moderate suppression. Acceptable diagnostic quality	Poor suppression. Unacceptable diagnostic quality	No distinction from background tissue

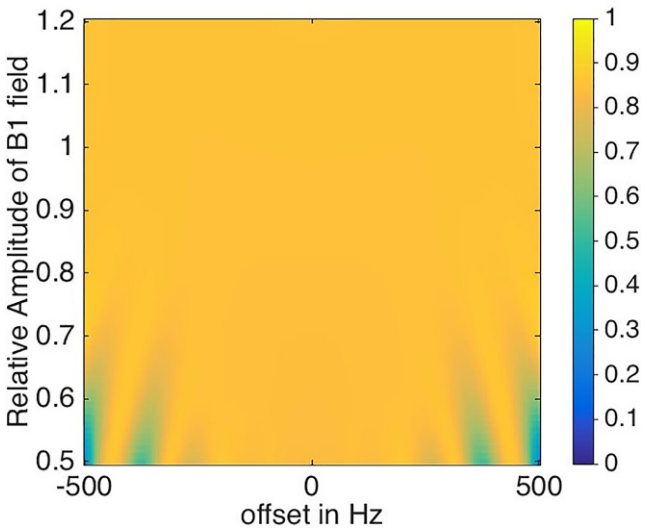

Fig. 2 Nerve signal simulation with Bloch as a function of B1 offset for the used B1-insensitive rotation (BIR-4) pulse. Nerve signal simulated with Bloch as a function of B1 offset for the used BIR-4 pulse. The pulse is expected to be robust in the presence of B1 offsets up to approximately 500 Hz for even small relative B1 amplitudes

Evaluation of the quality of maximum intensity projection (MIP) images was performed independently by two radiologists (E. K., N. S. with 3 and 2 years of experience in MR neurography, respectively). The readers were blinded to the clinical information of the patients, sequence parameters and the final radiological reports of MR neurography. The following categories were scored using a five-point grading scale (see Table 1): overall image quality, overall artifacts, vessel artifacts within plexus region, plexus signal homogeneity, visibility of small nerve branches, contrast of nerve to surrounding tissue, arterial suppression and venous suppression.

Statistical Analysis

Data were analyzed using IBM SPSS Statistics v. 23 (Armonk, NY, USA). Rating scores were compared between the sequences and statistically analyzed by using the non-parametric Wilcoxon signed-rank test. Interobserver agreement was determined by measuring the intraclass correlation coefficients (ICCs) for the two methods for each criterion. The ICC model was based on a two-way random comparison of absolute agreement type and the coefficients were computed with a significance level of 5%. Paired Student's t-tests were used to assess the differences in signal to noise intensity ratios and contrast to noise ratios between both STIR sequences on the same patient. *p*-values of less than 0.05 were taken as statistically significant.

Results

As illustrated in Fig. 2, signal simulations show the robustness of the used BIR-4 pulse in the presence of B1 offsets up to approximately 500 Hz for imaging nerves in a wide range of B1 amplitudes (0.5–1.5 of the nominal B1 value).

Targeted MIP images of the brachial plexus of two representative patients are shown in Figs. 3 and 4. Both STIR 3D TSE and STIR iMSDE 3D TSE sequences show uniform homogeneous fat suppression in the entire cervical area. The iMDSE prepulse results in suppression of the arterial as well as venous vessel signal enhancing the visualization of nerve structures, which become particularly obvious in regions with an immediate proximity of blood vessels to the plexus nerves, e. g. clavicular region (see enlarged insert).

Compared to STIR 3D TSE, STIR iMSDE 3D TSE yielded significantly higher aNMCNRs in the center and

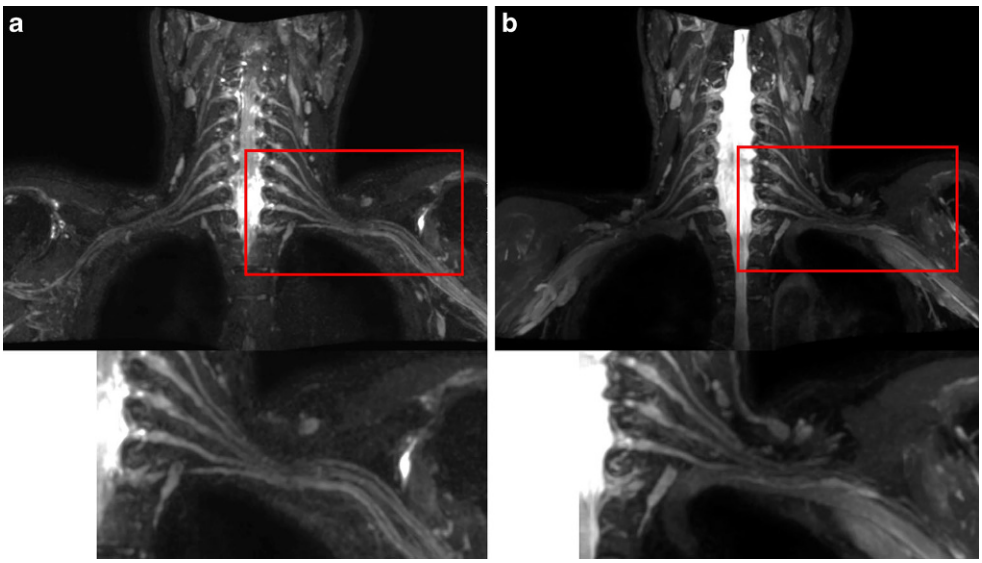

Fig. 3 MIP images of the brachial plexus of one representative patient. **a** STIR iMSDE 3D-TSE. **b** STIR 3D TSE. The additional adiabatic T2 preparation incorporating iMSDE-based motion sensitization prepulse reveals a good suppression of the arterial and venous vessel signal (**a**), which becomes particularly obvious in regions with an immediate proximity of blood vessels to the plexus nerves (e. g. clavicular region, see enlarged insert in **a**)

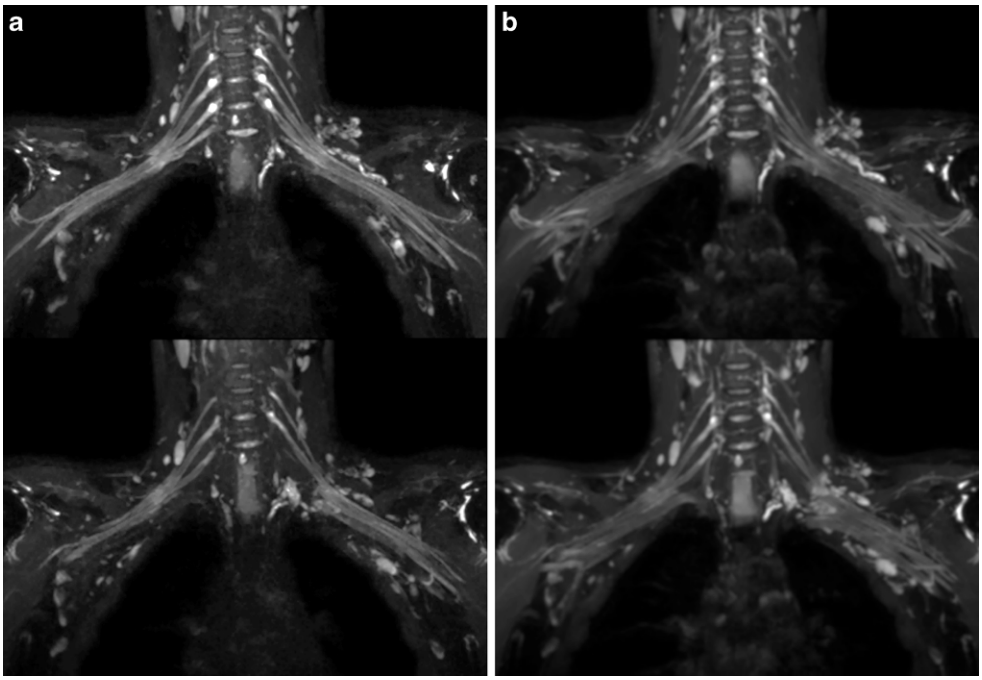

Fig. 4 Targeted MIP images of the brachial plexus in a patient suffering from paresthesia and weakness of the left arm. Images were acquired with STIR iMSDE 3D TSE (**a**) and STIR 3D TSE (**b**) showing a hyperintense multicystic lesion walling in the fascicles of the left brachial plexus. Without iMSDE prepulse (**b**), the vessel signal confounds the visualization of the nerves

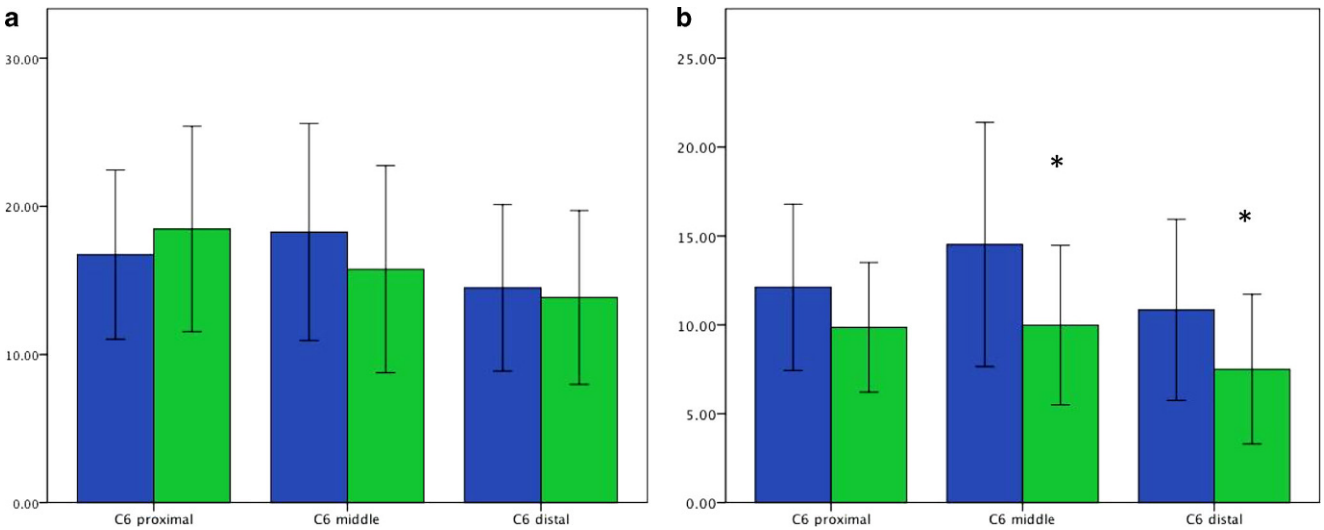

Fig. 5 Results of quantitative assessments measured on three different levels of the left C6 nerve (means ± standard deviations). **a** Apparent signal to noise ratio (aSNR), defined as ratio of signal mean to its standard deviation. **b** Apparent nerve-muscle contrast to noise ratio (aNMCNR) defined as signal mean nerve minus signal mean adjacent soft tissue divided by standard deviation of nerve signal. *blue* STIR iMSDE 3D TSE, *green* STIR 3D TSE, * denotes statistical significant differences ($p < 0.05$)

distal part (close proximity to vessels) of the left brachial plexus following the C6 nerve (14.5 ± 6.9 vs. 9.9 ± 4.5, $p = 0.013$; 10.9 ± 5.1 vs. 7.5 ± 4.2, $p = 0.038$) and a tendency for higher aNMCNR in the proximal part (12.1 ± 4.7 vs. 9.8 ± 3.6, $p = 0.084$); no significant differences were found for aSNR between both sequences (Fig. 5).

Furthermore, STIR iMSDE 3D TSE yielded significantly higher aNVCNRs than STIR 3D TSE in the analyzed regions (STIR iMSDE 3D TSE: 13.27 ± 6.70 vs. STIR 3D TSE: 2.83 ± 6.45; $p < 0.001$).

The semiquantitative ratings of the two radiologists revealed a better overall image quality ($p = 0.001$), a higher contrast of nerve signal to surrounding tissue ($p < 0.001$), less overall artifacts ($p < 0.001$), less artifacts by vessel signal ($p < 0.001$), a higher arterial as well as a higher venous suppression (both $p < 0.001$) when examining the STIR iMSDE 3D TSE compared to the STIR 3D TSE. No significant differences were found regarding the visibility of small nerve structures and the signal homogeneity of the nerves (Fig. 6). The average ICC for interobserver agree-

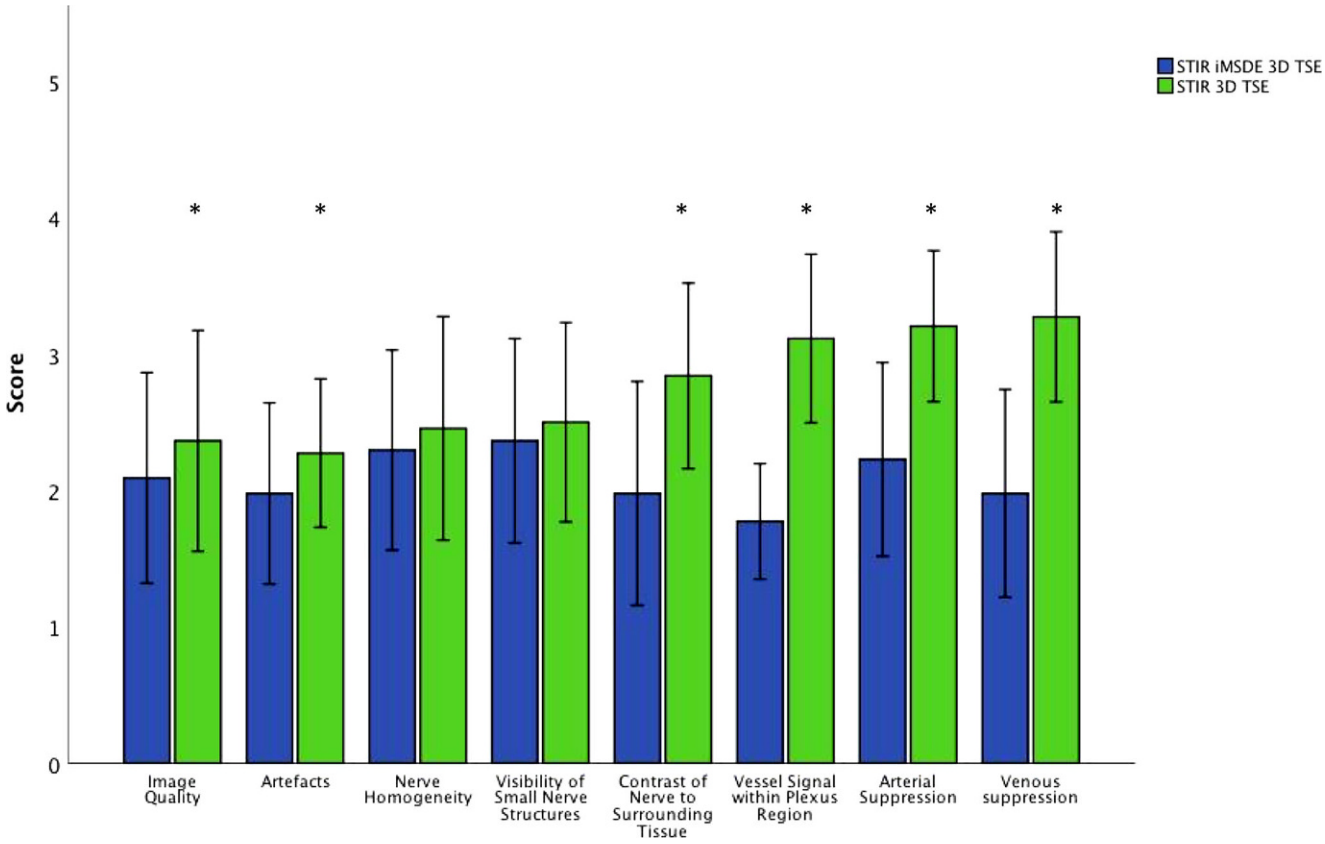

Fig. 6 Results of the semiquantitative ratings of the two radiologists. Results are reported as mean values ± standard deviations. *blue* STIR iMSDE 3D TSE, *green* STIR 3D TSE, * denotes statistical significant differences ($p < 0.05$), *p*-values refer to the results of the performed nonparametric Wilcoxon signed-rank test comparing the ratings between the two sequences

ment was 0.86 for STIR iMSDE 3D TSE and 0.82 for STIR 3D TSE.

Discussion

In the present study we evaluated a STIR 3D TSE sequence in conjunction with an adiabatic T2 and motion-sensitized preparation based on improved motion-sensitized driven equilibrium (STIR iMSDE 3D TSE) for MRN of the brachial plexus in a clinical routine setting. This sequence was compared with a STIR 3D TSE without motion sensitizing prepulse. It has been shown in previous studies that with help of the vascular signal suppression obtained by an iMSDE preparation the visualization of nerves can be improved in various anatomical settings [18–21]. The use of MR neurography of the brachial plexus, however, is still challenging due to its unique anatomy and therefore its sensitivity to B0 and B1 inhomogeneities for homogenous vessel suppression across the complete field of view [27]. These basic problems exist at all field strengths; nevertheless, they are more pronounced at higher magnetic field intensity due to the increased magnitude of B0 and B1 inhomogeneities. The applied iMSDE sequence module was based on a modified BIR-4 pulse, which has been expected to be robust against these inhomogeneities occurring in the shoulder-neck region for nerve imaging in a wide range of B1 amplitudes leading to a stable 3D T2w imaging.

The STIR 3D TSE and STIR iMSDE 3D TSE procedures were shown to provide robust high-quality fat-suppressed T2w imaging of brachial plexus nerves. The homogeneous fat suppression delivered by the wide-band STIR pulse employed resulted in good soft tissue contrast that, in combination with high spatial resolution, yielded the image quality necessary for the adequate assessment of the plexus anatomy, plexopathies and peripheral neuropathies. The additional iMSDE prepulse resulted in uniform arterial and venous signal suppressions, enhancing the visualization of the nerve structures of the brachial plexus in clinically feasible imaging times. The present qualitative results therefore lead to improved diagnostic reliability and accuracy regarding different plexopathies, which can be a major difficulty encountered even by experienced musculoskeletal radiologists. The quantitative analyses resulted in STIR iMSDE 3D TSE having significantly higher aCNRs without significant decrease in SNR, especially in the sections with

a close proximity of the nerves to vascular structures. This can be explained by improved nerve to vessel contrast resulting from vessel suppression. Furthermore, higher nerve to muscle contrast is caused by a stronger T2 weighting due to a longer effective echo time with the inclusion of the adiabatic iMSDE prepulse. Semiquantitative ratings performed by two clinical radiologists resulted in a better overall image quality, higher contrast of nerve signal to surrounding tissue, less overall artifacts, less artifacts by vessel signal, better arterial as well as better venous suppression for the implemented iMSDE prepulse. Given the identical spatial resolution used by the two compared sequences, no differences were found regarding the visibility of small nerve branches. Furthermore, nerve signal homogeneity was comparable between STIR 3D TSE and STIR iMSDE 3D TSE.

Our study has several limitations. Because only a small number of patients were examined ($N = 22$), this sequence needs further validation in larger cohorts. Additional clinical studies are required to validate the benefits of this fat and vessel-suppressed sequence in the evaluation of different pathologic conditions involving the brachial plexus, such as tumors, traumatic lesions and inflammatory changes. Furthermore, diagnostic comparisons to other MRN techniques should be performed in forthcoming studies; especially a sequence comparison with the recently introduced modified multi-echo Dixon 3D TSE should be considered [26]. This sequence also provides a robust fat suppression and uses a modified 3D TSE flip angle train for blood signal suppression, which can however increase the overall motion sensitivity of the acquisition.

In conclusion, the presented adiabatic iMSDE-prepared STIR 3D TSE method was shown to provide robust high-quality fat-suppressed 3D T2w imaging of brachial plexus nerves in the presence of B0 and B1 inhomogeneities in a clinically feasible imaging time. The incorporation of iMSDE-based motion sensitization results in robust blood suppression of vessels in close proximity to the brachial plexus nerves, leading to a higher contrast to noise ratio, an increased conspicuousness of the nerves, a better image quality and fewer artifacts. Therefore, STIR iMSDE 3D TSE can be considered for clinical MRN examinations of the brachial plexus.

Funding The present work was partially supported by Philips Healthcare and the European Union (ERC-StG 2014 iBack).

Conflict of interest E. Klupp, B. Cervantes, N. Sollmann, F. Treibel, D. Weidlich, T. Baum, E.J. Rummeny, C. Zimmer, J.S. Kirschke and D.C. Karampinos declare that they have no competing interests.

References

1. Joint Task Force of the EFNS and the PNS. European Federation of Neurological Societies/Peripheral Nerve Society guideline on management of multifocal motor neuropathy. Report of a joint task force of the European Federation of Neurological Societies and the Peripheral Nerve Society--first revision. J Peripher Nerv Syst. 2010;15:295–301.
2. Joint Task Force of the EFNS and the PNS.European Federation of Neurological Societies/Peripheral Nerve Society Guideline on management of paraproteinemic demyelinating neuropathies. Report of a Joint Task Force of the European Federation of Neurological Societies and the Peripheral Nerve Society--first revision. J Peripher Nerv Syst. 2010;15:185–95.
3. Joint Task Force of the EFNS and the PNS. European Federation of Neurological Societies/Peripheral Nerve Society Guideline on management of chronic inflammatory demyelinating polyradiculoneuropathy: report of a joint task force of the European Federation of Neurological Societies and the Peripheral Nerve Society--First Revision. J Peripher Nerv Syst. 2010;15:1–9.
4. Gooch CL, Weimer LH. The electrodiagnosis of neuropathy: basic principles and common pitfalls. Neurol Clin. 2007;25:1–28.
5. Du R, Auguste KI, Chin CT, Engstrom JW, Weinstein PR. Magnetic resonance neurography for the evaluation of peripheral nerve, brachial plexus, and nerve root disorders. J Neurosurg. 2010;112:362–71.
6. Martinoli C, Gandolfo N, Perez MM, Klauser A, Palmieri F, Padua L, Tagliafico A. Brachial plexus and nerves about the shoulder. Semin Musculoskelet Radiol. 2010;14:523–46.
7. Tagliafico A, Succio G, Emanuele Neumaier C, Serafini G, Ghidara M, Calabrese M, Martinoli C. MR imaging of the brachial plexus: comparison between 1.5-T and 3-T MR imaging: preliminary experience. Skeletal Radiol. 2011;40:717–24.
8. Chhabra A, Lee PP, Bizzell C, Soldatos T. 3 tesla MR neurography—technique, interpretation, and pitfalls. Skeletal Radiol. 2011;40:1249–60.
9. Hiwatashi A, Togao O, Yamashita K, Kikuchi K, Ogata H, Yamasaki R, Yoneyama M, Kira JI, Honda H. Evaluation of chronic inflammatory demyelinating polyneuropathy: 3D nerve-sheath signal increased with inked rest-tissue rapid acquisition of relaxation enhancement imaging (3D SHINKEI). Eur Radiol. 2017;27:447–53.
10. Schwarz D, Kele H, Kronlage M, Godel T, Hilgenfeld T, Bendszus M, Bäumer P. Diagnostic value of magnetic resonance neurography in cervical radiculopathy: plexus patterns and peripheral nerve lesions. Invest Radiol. 2018;53:158–66.
11. Gerevini S, Agosta F, Riva N, Spinelli EG, Pagani E, Caliendo G, Chaabane L, Copetti M, Quattrini A, Comi G, Falini A, Filippi M. MR imaging of brachial plexus and limb-girdle muscles in patients with amyotrophic lateral sclerosis. Radiology. 2016;279:553–61.
12. Madhuranthakam AJ, Lenkinski RE. Technical advancements in MR neurography. Semin Musculoskelet Radiol. 2015;19:86–93.
13. Viallon M, Vargas MI, Jlassi H, Lövblad KO, Delavelle J. High-resolution and functional magnetic resonance imaging of the brachial plexus using an isotropic 3D T2 STIR (Short Term Inversion Recovery) SPACE sequence and diffusion tensor imaging. Eur Radiol. 2008;18:1018–23.
14. Vargas MI, Viallon M, Nguyen D, Beaulieu JY, Delavelle J, Becker M. New approaches in imaging of the brachial plexus. Eur J Radiol. 2010;74:403–10.
15. Chhabra A, Thawait GK, Soldatos T, Thakkar RS, Del Grande F, Chalian M, Carrino JA. High-resolution 3T MR neurography of the brachial plexus and its branches, with emphasis on 3D imaging. AJNR Am J Neuroradiol. 2013;34:486–97.
16. Oudeman J, Coolen BF, Mazzoli V, Maas M, Verhamme C, Brink WM, Webb AG, Strijkers GJ, Nederveen AJ. Diffusion-prepared neurography of the brachial plexus with a large field-of-view at 3T. J Magn Reson Imaging. 2016;43:644–654.

17. Chhabra A, Zhao L, Carrino JA, Trueblood E, Koceski S, Shteriev F, Lenkinski L, Sinclair CD, Andreisek G. MR neurography: advances. Radiol Res Pract. 2013;2013:809568.
18. Cervantes B, Kirschke JS, Klupp E, Kooijman H, Börnert P, Haase A, Rummeny EJ, Karampinos DC. Orthogonally combined motion- and diffusion-sensitized driven equilibrium (OC-MDSDE) preparation for vessel signal suppression in 3D turbo spin echo imaging of peripheral nerves in the extremities. Magn Reson Med. 2018;79:407–415.
19. Kasper JM, Wadhwa V, Scott KM, Rozen S, Xi Y, Chhabra A. SHINKEI—a novel 3D isotropic MR neurography technique: technical advantages over 3DIRTSE-based imaging. Eur Radiol. 2015;25:1672–7.
20. Yoneyama M, Nakumara M, Okukari T, Tabuchi T, Takemura A, Obara M, Ogura J. High-resolution 3D volumetric nerve-sheath weighted RARE imaging (3D SHINKEI). In: Proceedings of the 19th annual meeting of ISMRM. 2011. p. 2721.
21. Yoneyama M, Takahara T, Kwee TC, Nakamura M, Tabuchi T. Rapid high resolution MR neurography with a diffusion-weighted pre-pulse. Magn Reson Med Sci. 2013;12:111–9.
22. Jenista ER, Rehwald WG, Chen EL, Kim HW, Klem I, Parker MA, Kim RJ. Motion and flow insensitive adiabatic T2-preparation module for cardiac MR imaging at 3 Tesla. Magn Reson Med. 2013;70:1360–8.
23. Nezafat R, Ouwerkerk R, Derbyshire AJ, Stuber M, McVeigh ER. Spectrally selective B1-insensitive T2 magnetization preparation sequence. Magn Reson Med. 2009;61:1326–35.
24. Weidlich D, Schlaeger S, Kooijman H, Börnert P, Kirschke JS, Rummeny EJ, Haase A, Karampinos DC. T2 mapping with magnetization-prepared 3D TSE based on a modified BIR-4 T2 preparation. NMR Biomed. Epub 2017 Aug 4.
25. Cervantes B. High-resolution DWI of the lumbar plexus using B1-insensitive velocity-compensated diffusion-prepared 3D TSE. In: Proceedings of the 24th annual meeting of ISMRM. 2016.
26. Wang X, Harrison C, Mariappan YK, Gopalakrishnan K, Chhabra A, Lenkinski RE, Madhuranthakam AJ. MR neurography of brachial plexus at 3.0 T with robust fat and blood suppression. Radiology. 2017;283:538–46.
27. Mürtz P, Kaschner M, Lakghomi A, Gieseke J, Willinek WA, Schild HH, Thomas D. Diffusion-weighted MR neurography of the brachial and lumbosacral plexus: 3.0 T versus 1.5 T imaging. Eur J Radiol. 2015;84:696–702.